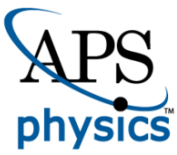

Unifying Microscopic and Continuum Treatments of van der Waals and Casimir Interactions

Prashanth S. Venkataram, Jan Hermann, Alexandre Tkatchenko, and Alejandro W. Rodriguez

Phys. Rev. Lett. **118**, 266802 — Published 29 June 2017

DOI: 10.1103/PhysRevLett.118.266802

Unifying microscopic and continuum treatments of van der Waals and Casimir interactions

Prashanth S. Venkataram,[1] Jan Hermann,[2] Alexandre Tkatchenko,[2,3] and Alejandro W. Rodriguez[1]

[1]*Department of Electrical Engineering, Princeton University, Princeton, New Jersey 08544, USA*
[2]*Fritz-Haber-Institut der Max-Planck-Gesellschaft, Faradayweg 4–6, 14195, Berlin, Germany*
[3]*Physics and Materials Science Research Unit, University of Luxembourg, L-1511 Luxembourg*

(Dated: May 31, 2017)

We present an approach for computing long-range van der Waals (vdW) interactions between complex molecular systems and arbitrarily shaped macroscopic bodies, melding atomistic treatments of electronic fluctuations based on density functional theory in the former, with continuum descriptions of strongly shape-dependent electromagnetic fields in the latter, thus capturing many-body and multiple scattering effects to all orders. Such a theory is especially important when considering vdW interactions at mesoscopic scales, i.e. between molecules and structured surfaces with features on the scale of molecular sizes, in which case the finite sizes, complex shapes, and resulting nonlocal electronic excitations of molecules are strongly influenced by electromagnetic retardation and wave effects that depend crucially on the shapes of surrounding macroscopic bodies. We show that these effects together can modify vdW interaction energies and forces, as well as molecular shapes deformed by vdW interactions, by orders of magnitude compared to previous treatments based on Casimir–Polder, nonretarded, or pairwise approximations, which are valid only at macroscopically large or atomic-scale separations or in dilute insulating media, respectively.

Van der Waals (vdW) interactions play an essential role in non-covalent phenomena throughout biology, chemistry, and condensed-matter physics [1–3]. It has long been known that vdW interactions among a system of polarizable atoms are not pairwise-additive but instead strongly depend on geometric and material properties [2, 4, 5]. However, only recently developed theoretical methods have made it possible to account for short-range quantum interactions in addition to long-range many-body screening in molecular ensembles [3, 6–15], demonstrating that nonlocal many-body effects cannot be captured by simple, pairwise-additive descriptions; these calculations typically neglect electromagnetic retardation effects in molecular systems. Simultaneously, recent theoretical and experimental work has characterized dipolar Casimir–Polder interactions between macroscopic metallic or dielectric objects and atoms, molecules, or Bose–Einstein condensates, further extending to nonzero temperatures, dynamical situations, and fluctuations in excited states (as in so-called Rydberg atoms) [16–25]. Yet, while theoretical treatments have thus far accounted for the full electrodynamic response of macroscopic bodies (including retardation), they often treat molecules as point dipoles of some effective bulk permittivities or as collections of noninteracting atomic dipoles, ignoring finite size and other many-body electromagnetic effects.

In this paper, motivated by the aforementioned theoretical developments [1, 16–18, 24–28], we describe an approach that seamlessly connects atomistic descriptions of large molecules to continuum descriptions of *arbitrary* macroscopic bodies, characterizing their mutual vdW interactions. In particular, while molecules in proximity with macroscopic objects require atomistic descriptions of the latter, and large molecules far from macroscopic objects require consideration of contributions from vibrational (in addition to electronic) resonances to the vdW interaction energy, we focus on a mesoscopic regime involving molecular sizes and separations on the order of 1–100 nm, where macroscopic objects can be treated continuously for the purposes of computing electromagnetic field responses (and molecular vibrational resonances can be neglected), yet electromagnetic retardation in conjunction with the finite sizes, nontrivial shapes, and nonlocal electronic correlations of large molecules need to be self-consistently considered to accurately characterize vdW interactions. We specifically investigate interactions among various large molecules and gold surfaces, and show that the effect of nonlocal polarization correlations, encapsulated in the ratio of retarded, many-body (RMB) to pairwise vdW energies (or forces), causes relative deviations from pairwise treatments ranging from 20% to over 3 orders of magnitude. Further quantitative differences of over an order of magnitude, along with additional qualitative deviations when considering vdW-driven deformations of elongated molecules above conducting surfaces, are observed when retardation or finite size effects are neglected.

Our work is based on an equation for the long-range dispersive vdW energy of a system of polarizable bodies, consisting of N microscopic bodies (molecules), labeled by k and described by electric susceptibilities $\mathbb{V}_k$, and a collection of continuum bodies (an environment) described by a collective, macroscopic susceptibility $\mathbb{V}_{\mathrm{env}}$, displayed schematically in Fig. 1. The energy of such a collection of bodies can be obtained from the scattering framework [29] and written as an integral over imaginary frequency $\omega = \mathrm{i}\xi$,

$$\mathcal{E} = \frac{\hbar}{2\pi}\int_0^\infty \mathrm{d}\xi\ \ln[\det(\mathbb{T}_\infty \mathbb{T}^{-1})], \tag{1}$$

in terms of T-operators that depend on the bodies' susceptibilities as well as on the homogeneous electric Green's function $\mathbb{G}_0(\mathrm{i}\xi,\mathbf{x},\mathbf{x}') = (\nabla\otimes\nabla - \frac{\xi^2}{c^2}\mathbb{I})\frac{e^{-\frac{\xi|\mathbf{x}-\mathbf{x}'|}{c}}}{4\pi|\mathbf{x}-\mathbf{x}'|}$ (including retardation) mediating electromagnetic interactions; they encode the scattering properties of the various bodies, and are given by,

$$\mathbb{T} = \left(\mathbb{I} - (\mathbb{V}+\mathbb{V}_{\mathrm{env}})\mathbb{G}_0\right)^{-1}(\mathbb{V}+\mathbb{V}_{\mathrm{env}}),$$

where $\mathbb{V} = \sum_k \mathbb{V}_k$; $\mathbb{T}_\infty = \mathbb{T}_{\rm env} \prod_k \mathbb{T}_k$, written in terms of $\mathbb{T}_{k({\rm env})} = (\mathbb{I} - \mathbb{V}_{k({\rm env})}\mathbb{G}_0)^{-1}\mathbb{V}_{k({\rm env})}$, encodes the scattering response of the bodies in isolation from one another [29]. Though this framework treats molecular and macroscopic susceptibilities equally, since microscopic and macroscopic bodies are assumed to be disjoint, it is more efficient to partition the T-operators into blocks belonging to either molecules or macroscopic objects, allowing a trace over the macroscopic degrees of freedom (DOFs). The definitions of $\mathbb{T}_{k({\rm env})}$ imply $\mathbb{T}^{-1}_{k({\rm env})} = \mathbb{V}^{-1}_{k({\rm env})} - \mathbb{G}_0$, which means that the relevant T-operators can be written as:

$$\mathbb{T}^{-1} = \begin{bmatrix} \mathbb{T}^{-1}_{\rm mol} & -\mathbb{G}_0 \\ -\mathbb{G}_0 & \mathbb{T}^{-1}_{\rm env} \end{bmatrix}, \quad \mathbb{T}_\infty = \begin{bmatrix} \mathbb{T}_{{\rm mol},\infty} & 0 \\ 0 & \mathbb{T}_{\rm env} \end{bmatrix} \tag{2}$$

thus partitioning the molecular and macroscopic (environmental) DOFs. These depend on the molecular T-operators

$$\mathbb{T}^{-1}_{\rm mol} = \begin{bmatrix} \mathbb{T}_1^{-1} & -\mathbb{G}_0 & \dots & -\mathbb{G}_0 \\ -\mathbb{G}_0 & \mathbb{T}_2^{-1} & \dots & -\mathbb{G}_0 \\ \vdots & \vdots & \ddots & \vdots \\ -\mathbb{G}_0 & -\mathbb{G}_0 & \dots & \mathbb{T}_N^{-1}, \end{bmatrix} \tag{3}$$

with $\mathbb{T}_{{\rm mol},\infty} = \prod_k \mathbb{T}_k$, which are in turn partitioned into blocks for each of the N molecular bodies. Given this, the product in the determinant can be evaluated as:

$$\begin{aligned} \det(\mathbb{T}_\infty \mathbb{T}^{-1}) &= \det(\mathbb{T}_{{\rm mol},\infty}\mathbb{T}^{-1}_{\rm mol}) \det(\mathbb{I} - \mathbb{G}_0\mathbb{T}_{\rm env}\mathbb{G}_0\mathbb{T}_{\rm mol}) \\ &= \det(\mathbb{T}_{{\rm mol},\infty}\mathbb{T}^{-1}_{\rm mol}) \det(\mathbb{I} - \mathbb{G}_{\rm env}\mathbb{V}) \\ &\quad \times \det(\mathbb{I} - \mathbb{G}_0\mathbb{V})^{-1} \end{aligned} \tag{4}$$

where we used the property $\mathbb{G}_0\mathbb{T}_{k({\rm env})} = (\mathbb{I} - \mathbb{G}_0\mathbb{V}_{k({\rm env})})^{-1} - \mathbb{I}$, and consolidated the scattering properties of the macroscopic bodies into the operator $\mathbb{G}_{\rm env} = \mathbb{G}_0(\mathbb{I} - \mathbb{V}_{\rm env}\mathbb{G}_0)^{-1}$, which solves Maxwell's equations

$$\left[\nabla \times \nabla \times + \frac{\xi^2}{c^2}\left(\mathbb{I} + \mathbb{V}_{\rm env}\right)\right] \mathbb{G}_{\rm env} = -\frac{\xi^2}{c^2}\mathbb{I} \tag{5}$$

for an imaginary frequency $\omega = {\rm i}\xi$, thereby encoding the macroscopic DOFs purely in the electric field response. Moreover, as the molecules are all disjoint, then $\det(\mathbb{T}_{{\rm mol},\infty}\mathbb{T}^{-1}_{\rm mol}) = \det(\mathbb{I} - \mathbb{G}_0\mathbb{V}) \prod_k \det(\mathbb{I} - \mathbb{G}_0\mathbb{V}_k)^{-1}$. Putting all of these identities together yields the following expression for the energy:

$$\mathcal{E} = \frac{\hbar}{2\pi}\int_0^\infty {\rm d}\xi \ \ln[\det\left(\mathbb{M}\mathbb{M}^{-1}_\infty\right)] \tag{6}$$

where $\mathbb{M} = \mathbb{I} - \mathbb{G}_{\rm env}\mathbb{V}$ and $\mathbb{M}_\infty = \prod_k(\mathbb{I} - \mathbb{G}_0\mathbb{V}_k)$.

Previous scattering treatments of (1) in Casimir physics have been restricted to continuum bodies [29], while previous microscopic fluctuation–dissipation treatments of (6) in vdW physics have been restricted to purely molecular bodies exhibiting nonretarded interactions in vacuum [8]. Having demonstrated the equivalence of (1) and (6) for arbitrary bodies (see [30] for an alternate equivalent derivation of (6) based on the fluctuation–dissipation theorem), we accurately describe the DOFs of molecular and continuum bodies interacting at nanometric and larger separations by seamlessly conjoining [31] recently-discussed ab-initio electronic density descriptions of molecular responses [3, 6, 8, 13] with state-of-the-art analytical or numerical techniques from continuum electrodynamics [1, 26–28]. In particular, classical electrodynamic techniques, including scattering [29, 32, 33] and finite-difference [34–36] methods, can be used to solve Maxwell's equations (5) and thereby express the macroscopic field response $\mathbb{G}_{\rm env}$ in a convenient basis, such as incoming and outgoing propagating planewaves, as is typical of the scattering framework [29], or via localized functions, e.g. tetrahedral mesh elements, in brute-force formulations [27, 33]. Microscopic bodies, on the other hand, generally require quantum descriptions, but recent work has shown that one can accurately represent their response $\mathbb{V}_k = \sum_p \alpha_p |f_p\rangle\langle f_p|$ through bases $\{|f_p\rangle\}$ of either exponentially localized (for insulators) or polynomially delocalized (for metals) functions [37], that accurately capture multipolar interactions among electronic wavefunctions [3, 6, 8, 13]. The microscopic and macroscopic DOFs, regardless of the specific choice of basis representation, come together in the operator products $\mathbb{G}\mathbb{V}_k$; when represented in the p-dimensional molecular basis $\{|f_p\rangle\}$, their block matrix elements are of the form:

$$\langle f_p|\mathbb{G}\mathbb{V}_k f_q\rangle = \alpha_q \int {\rm d}^3\mathbf{x}\, {\rm d}^3\mathbf{x}'\ f_p(\mathbf{x})\mathbb{G}(\mathbf{x},\mathbf{x}')f_q(\mathbf{x}') \tag{7}$$

(see [30] for more details). The particular molecules we consider have finite electronic gaps, allowing accurate description of the bare response via sums over dipolar ground-state oscillator densities [5, 8–10, 12, 14, 38],

$$f_p({\rm i}\xi,\mathbf{x}) = \left(\sqrt{2\pi}\sigma_p\left({\rm i}\xi\right)\right)^{-3} \exp\left(-\frac{(\mathbf{x}-\mathbf{x}_p)^2}{2\,\sigma_p^2\left({\rm i}\xi\right)}\right), \tag{8}$$

centered at the locations $\mathbf{x}_p$ of each atom p, normalized such that $\int {\rm d}^3\mathbf{x}\ f_p = 1$, and featuring a Gaussian width that, rather than being phenomenological [39, 40], depends on the atomic polarizability via $\sigma_p({\rm i}\xi) = \left(\frac{\alpha_p({\rm i}\xi)}{\sqrt{72\pi^3}}\right)^{1/3}$ [8, 41]. The isotropic

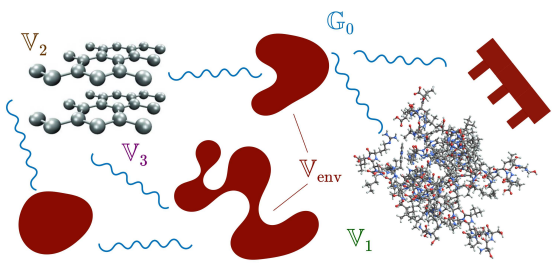

Figure 1. Schematic of molecular bodies described by electric susceptibilities $\mathbb{V}_n$ in the vicinity of and interacting with macroscopic bodies described by a collective susceptibility $\mathbb{V}_{\rm env}$, where the interactions are mediated by vacuum electromagnetic fields $\mathbb{G}_0$.

atomic polarizabilities α_p are computed via density functional theory, as in recent works [8, 9], which include short-range electrostatic, hybridization, and quantum exchange effects.

The log-determinant formula for the energy (6), for any basis representation of $\mathbb{M}$ & $\mathbb{M}_\infty$, includes retardation by construction and accounts for many-body screening and multiple scattering to all orders, thereby ensuring full consideration of finite size, complex shape effects, and collective polarization excitations owing to long-range electromagnetic interactions. We demonstrate the importance of all of these effects by comparing vdW energies (or forces) obtained from (6) to those from pairwise or other approximate treatments in a number of configurations, consisting of one or two molecules above either a gold half-space or a conical gold tip. While the Green's function of the half-space can be computed analytically [42], the latter is computed using brute-force numerical techniques [1, 26–28], with the dielectric function of gold taken from [16]. We specifically study a C_{500}-fullerene of radius 1 nm, a 250 atom 30 nm-long linear carbyne wire, and a 1944 atom-large 2.6 nm $\times$ 2.9 nm $\times$ 5.5 nm protein associated with human Huntington's disease [43–45].

We further compare the RMB energy from (6) to typical approximations used in the literature: the non-retarded vdW energy $\mathcal{E}_0$, obtained by evaluating (6) with $\mathbb{G}_0$ and $\mathbb{G}_{\rm env}$ replaced by their respective quasistatic ($c \to \infty$) responses, and the Casimir–Polder (CP) energy,

$$\mathcal{E}_{\rm CP} = -\frac{\hbar}{2\pi}\int_0^\infty {\rm d}\xi\ {\rm Tr}\left[\alpha\cdot\mathbb{G}_{\rm env}\cdot\left(\mathbb{I}+\frac{1}{2}\alpha\cdot\mathbb{G}_{\rm env}\right)\right] \tag{9}$$

which ignores finite size effects by instead contracting the dressed susceptibility of the molecular ensemble into effective dipolar polarizabilities,

$$\alpha = \bigoplus_k \sum_{p,q} \langle f_p|(\mathbb{I}-\mathbb{V}_k\mathbb{G}_0)^{-1}\mathbb{V}_k f_q\rangle,$$

thus neglecting higher-order many-body interactions among the different molecules and surfaces. Finally, we define a pairwise interaction energy,

$$\mathcal{E}_{\rm PWS} = -\frac{\hbar}{2\pi}\int_0^\infty {\rm d}\xi\ {\rm Tr}\left[\sum_k \mathbb{V}_k\mathbb{G}_{\rm env}\left(\mathbb{I}+\frac{1}{2}\sum_{l\neq k}\mathbb{V}_l\mathbb{G}_{\rm env}\right)\right] \tag{10}$$

which, as in (9), is obtained as a lowest-order expansion of (6) in the scattering; this captures both finite size and retardation but ignores all high-order many-body interactions, with the sums over k, l running over either individual or pairs of molecules. When comparing non-retarded and CP energies to their corresponding pairwise approximations, it suffices to take the quasistatic limit in (10) or to let $(\mathbb{I}-\mathbb{V}_k\mathbb{G}_0)^{-1} \to \mathbb{I}$ for the effective polarizability α in (9), respectively.

Figure 2(a) shows the RMB to pairwise energy ratio $\frac{\mathcal{E}}{\mathcal{E}_{\rm PWS}}$ of various configurations (insets), with the fullerene interaction (blue line) found to vary only slightly, attaining a maximum of 1.16 at $z \approx 10$ nm; such a small discrepancy stems

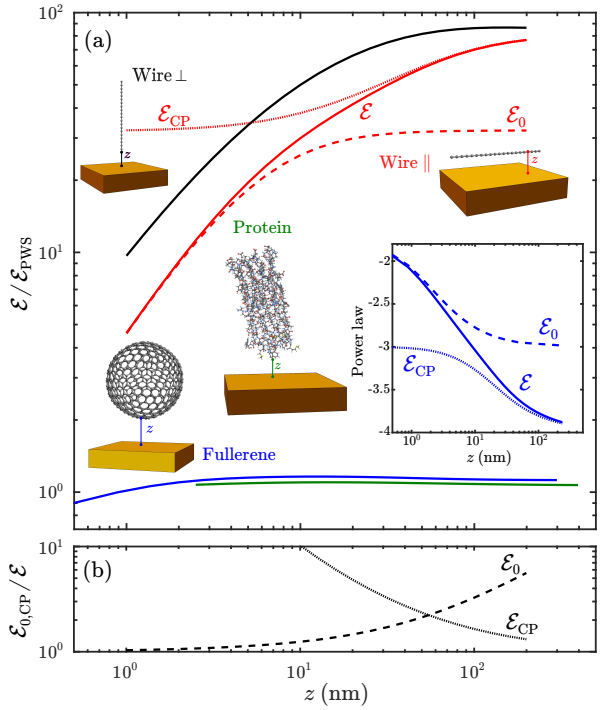

Figure 2. (a) Energy ratio $\frac{\mathcal{E}}{\mathcal{E}_{\rm PWS}}$ versus z for a fullerene (solid blue), protein (solid green), or wire in the parallel (solid red) or perpendicular (solid black) orientations, above the gold plate; $\mathcal{E}_{\rm PWS}$ is the energy obtained by a pairwise approximation defined in (10). Also shown are the predictions of both CP (dotted red) and non-retarded (dashed red) approximations for the case of a parallel wire. Inset: power law $\frac{\partial\ln(\mathcal{E})}{\partial\ln(z)}$ (solid blue) of the fullerene–plate system with respect to z, compared to both CP (dotted blue) and non-retarded (dashed blue) approximations. (b) CP $\mathcal{E}_{\rm CP}$ (dotted black) and non-retarded $\mathcal{E}_0$ (dashed black) energies of a perpendicular carbyne wire separated from a gold plate by a vertical distance z, normalized to the RMB energy $\mathcal{E}$ of (6), as a function of z

from the small size and isotropic shape of the fullerene, which limits possible nonlocal correlations in its polarization response. Even weaker relative correlations are observed in the case of the protein (green line), which despite its greater size, number of atoms, and chemical complexity, has a reduced response compared to semi-metallic carbon allotropes [8, 9]. To separate the various many-body effects, the inset of Fig. 2 compares the RMB power law $\frac{\partial\ln(\mathcal{E})}{\partial\ln(z)}$ of the fullerene interaction to its counterparts when neglecting either finite size or retardation. As expected, both approximations become accurate in their corresponding regimes of validity, with the power law asymptoting to -4 and -1.9 at large and small z, respectively, but fail in the intermediate, mesoscopic regime $z \approx 10$ nm. Even larger discrepancies arise in the case of the wire, whose large size and highly anisotropic shape support long-wavelength collective fluctuations. For the parallel wire [Fig. 2(a)] (red lines), the corresponding energy ratios behave differently in that the effect of screening is strongest in the quasistatic limit, which greatly dampens many-body excitations relative to pairwise approximations and hence leads to

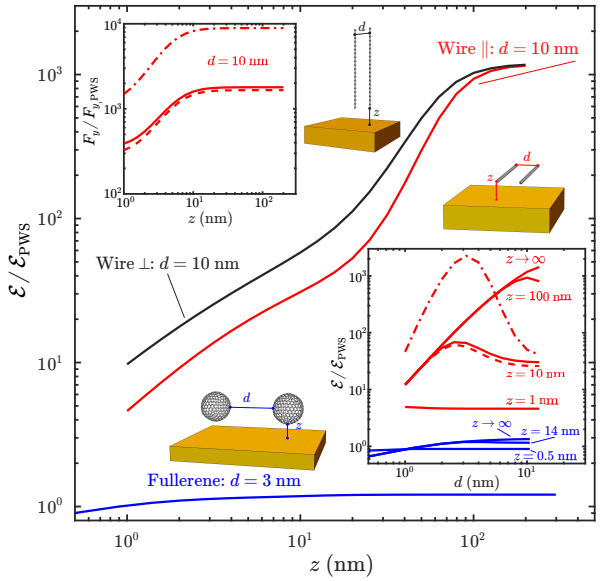

Figure 3. Energy ratio $\frac{\mathcal{E}}{\mathcal{E}_{\rm PWS}}$ versus vertical distance z for two fullerenes at fixed horizontal separation $d = 3$ nm (solid blue) or two wires at $d = 10$ nm, in either the parallel (solid red) or perpendicular (solid black) orientations, above a gold plate. Top inset: horizontal-force ratio $\frac{F_y}{F_{y,\rm PWS}}$ versus z for the parallel wires at $d = 10$ nm. Bottom inset: $\frac{\mathcal{E}}{\mathcal{E}_{\rm PWS}}$ versus d for the fullerenes and the parallel wires at several values of z; also shown are the corresponding ratios obtained via CP (dot-dashed red) and non-retarded (dashed red) approximations, specifically for $z = 10$ nm.

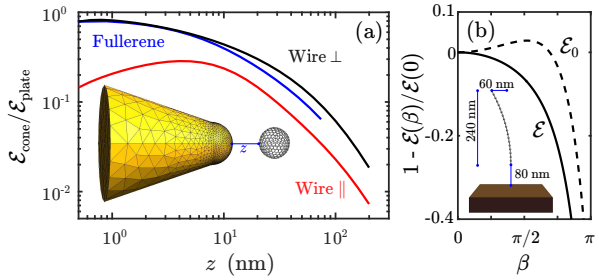

Figure 4. (a) Energy $\mathcal{E}_{\rm cone}$ of either a fullerene (solid blue) or carbyne wire (solid red/black) above a gold cone, normalized to the energy $\mathcal{E}_{\rm plate}$ of the same molecule but separated from a gold plate by the same surface–surface vertical distance z. (b) Energy variations $1 - \frac{\mathcal{E}(\beta)}{\mathcal{E}(0)}$, with (solid black) or without (dashed black) retardation, for a clamped long vertical carbyne wire as a function of dimensionless curvature β. Inset schematically shows the wire shape for $\beta = 0.5$.

smaller non-retarded energy ratios; in contrast, by construction CP ignores many-body interactions with the surface and thus screening has a much weaker impact relative to the pairwise approximation, leading to larger CP energy ratios. At intermediate $z \approx 10$ nm of the order of the wire length, $\mathcal{E}/\mathcal{E}_{\rm PWS} \approx 30$, with the approximate energy ratios deviating by 20%. Similar results are observed in the case of a wire in the perpendicular orientation (black lines), with the pairwise energy leading to slightly larger discrepancies at short separations due to the screening and decreasing impact of atoms farther away from the plate. We further find that the absolute values of both $\mathcal{E}_0$ (dashed black) and $\mathcal{E}_{\rm CP}$ (dotted black) for the perpendicular wire overestimate $\mathcal{E}$ by factors of over 2 [Fig. 2(b)] for $z > 10$ nm due to the slower decay of the Green's function in the former and lack of screening over the length (or modes) of the wire in the latter.

We now investigate the mutual vdW interactions among two fullerenes or parallel wires oriented either parallel or perpendicular to the gold plate [Fig. 3], focusing primarily on horizontal separations d on the order of molecular sizes, where many-body and finite size effects are strongest. Especially in the case of two wires, the pairwise approximation is shown to fail by many orders of magnitude, with the largest energy ratios occurring at asymptotically large z, i.e. for two molecules in vacuum, while at small z a decreasing ratio reflects the dominant interactions (and screening) of the individual molecules with the plate. The transition and competition between the two limiting behaviors occurs at mesoscopic $z \sim d$, and is more clearly visible from the plots in Fig. 3(lower inset), which show $\frac{\mathcal{E}}{\mathcal{E}_{\rm PWS}}$ versus d at several values of z. In particular, in the case of parallel wires at mesoscopic $z = 10$ nm, the competition leads to a nonmonotonic energy ratio, with the maximum of 70 occurring at intermediate $d \approx 3$ nm. Comparisons against non-retarded and CP approximations illustrate behaviors similar to the previous case of a single wire, with each under- or over-estimating the ratios by approximately 20% or 30%, respectively. Also shown in Fig. 3(upper inset) is the ratio of the physically observable horizontal force $F_y = -\frac{\partial \mathcal{E}}{\partial y}$ on the wires to its pairwise counterpart, plotted against z for parallel wires at $d = 10$ nm. Note that by construction, $F_{y,\rm PWS}$ is independent of z and thus, the system experiences an absolute decrease in the force due to the screening induced by the plate. Comparing $F_{y,0}$ and $F_{y,\rm CP}$, we find the surprising result that in contrast to the energies of a single molecule, the screening by the plate makes retardation more rather than less relevant to the force at small z, leading to an $\approx 10\%$ decrease in the force magnitude.

Finally, we consider more complex molecular and macroscopic geometries; we start with the energy of a molecule above a gold conical tip [Fig. 4(a)] by comparing it to that of a gold plate at the same vertical separation z, with $\mathbb{G}_{\rm env}$ in the former computed through the use of a free, surface-integral Maxwell solver, SCUFF-EM [46, 47]. The *finite* cone has a base diameter of 54 nm and a height of 50 nm from the base to the bottom of a hemispherical tip of diameter 20 nm. The ratios decrease with increasing z as the finite molecules sample first the slope and then the finite size of the cone, leading to the dipolar limit. At small z, the fullerene and perpendicular wire interact primarily with the proximate surface of the tip, so the ratios approach 1 as in a proximity approximation. By contrast, the ratio for a parallel wire is nonmonotonic, decreasing with z at short separations since in this configuration, the wire excitations in the limit $z \to 0$ still sample the finite curvature of the tip and conical slope. Next, we consider the

impact of retardation on the deformation of a longer carbyne wire of length $l = 240$ nm oriented vertically at $z = 80$ nm above a perfectly conducting plane [Fig. 4(b)]. For illustration, we consider wire shapes parameterized along the wire length by the angle $\theta(s) = \frac{\pi}{2} - \beta\frac{s}{l}$, where $\beta \geq 0$ represents a dimensionless curvature, thereby enforcing a fixed wire length and vertical slope at the bottom of the wire. We find, quite surprisingly, that while the retarded energy decreases monotonically with increasing β, as expected from a wire that curves toward the plane, the nonretarded energy exhibits the opposite behavior in the range $0 < \beta \lesssim \frac{\pi}{2}$, demonstrating the dramatic impact that retardation can have in this geometry; with more complex parameterizations $\theta(s)$, one could for instance study the impact of retardation on vdW-driven molecular deformations and wetting transitions near macroscopic bodies.

In conclusion, we have demonstrated a unifying approach to computing vdW interactions among molecules and macroscopic bodies that accounts for many-body and multiple-scattering effects to all orders. By comparing against commonplace pairwise, CP, and non-retarded approximations, we quantified the impact of nonlocality, finite size, and retardation on the vdW energy between molecules and either a planar or conical macroscopic body. We have consistently found larger deviations in approximate interactions for long, semimetallic molecules such as carbyne wires, whereas compact, insulating molecules such as many proteins are reasonably well-described as effectively dilute dielectric particles, allowing these low-order approximations to be more valid. In the future, one might consider more complex macroscopic bodies, such as periodic gratings [17, 18] that may elicit larger differences between RMB and approximate interactions even for compact biomolecules, as well as extend these results to incorporate the effects of infrared molecular resonances [16].

[1] L. M. Woods, D. A. R. Dalvit, A. Tkatchenko, P. Rodriguez-Lopez, A. W. Rodriguez, and R. Podgornik, Rev. Mod. Phys. **88**, 045003 (2016).

[2] D. Langbein, "Theory of van der waals attraction," in *Springer Tracts in Modern Physics* (Springer Berlin Heidelberg, Berlin, Heidelberg, 1974) pp. 1–139.

[3] A. Tkatchenko, Advanced Functional Materials **25** (2015).

[4] A. D. McLachlan, Molecular Physics **6**, 423 (1963).

[5] M. W. Cole, D. Velegol, H.-Y. Kim, and A. A. Lucas, Molecular Simulation **35**, 849 (2009).

[6] A. Tkatchenko, A. Ambrosetti, and R. A. DiStasio Jr., The Journal of Chemical Physics **138** (2013).

[7] V. V. Gobre and A. Tkatchenko, Nature Communications **4** (2013).

[8] R. A. DiStasio Jr., V. V. Gobre, and A. Tkatchenko, Journal of Physics: Condensed Matter **26**, 213202 (2014).

[9] A. Ambrosetti, N. Ferri, R. A. DiStasio, Jr., and A. Tkatchenko, Science **351**, 1171 (2016).

[10] A. D. Phan, L. M. Woods, and T.-L. Phan, Journal of Applied Physics **114** (2013).

[11] A. M. Reilly and A. Tkatchenko, Chem. Sci. **6**, 3289 (2015).

[12] Y. V. Shtogun and L. M. Woods, The Journal of Physical Chemistry Letters **1**, 1356 (2010).

[13] A. Ambrosetti, A. M. Reilly, R. A. DiStasio, and A. Tkatchenko, The Journal of Chemical Physics **140** (2014).

[14] H.-Y. Kim, J. O. Sofo, D. Velegol, M. W. Cole, and A. A. Lucas, Langmuir **23**, 1735 (2007).

[15] A. Tkatchenko, R. A. DiStasio Jr., R. Car, and M. Scheffler, Phys. Rev. Lett. **108**, 236402 (2012).

[16] S. Y. Buhmann, S. Scheel, S. A. Ellingsen, K. Hornberger, and A. Jacob, Phys. Rev. A **85**, 042513 (2012).

[17] S. Y. Buhmann, V. N. Marachevsky, and S. Scheel, International Journal of Modern Physics A **31**, 1641029 (2016).

[18] H. Bender, C. Stehle, C. Zimmermann, S. Slama, J. Fiedler, S. Scheel, S. Y. Buhmann, and V. N. Marachevsky, Phys. Rev. X **4**, 011029 (2014).

[19] P. Thiyam, C. Persson, B. E. Sernelius, D. F. Parsons, A. Malthe-Srenssen, and M. Boström, Phys. Rev. E **90**, 032122 (2014).

[20] P. Barcellona, R. Passante, L. Rizzuto, and S. Y. Buhmann, Phys. Rev. A **93**, 032508 (2016).

[21] F. Intravaia, C. Henkel, and M. Antezza, "Fluctuation-induced forces between atoms and surfaces: The casimir–polder interaction," in *Casimir Physics*, edited by D. Dalvit, P. Milonni, D. Roberts, and F. da Rosa (Springer Berlin Heidelberg, Berlin, Heidelberg, 2011) pp. 345–391.

[22] M. DeKieviet, U. D. Jentschura, and G. Łach, "Modern experiments on atom-surface casimir physics," in *Casimir Physics*, edited by D. Dalvit, P. Milonni, D. Roberts, and F. da Rosa (Springer Berlin Heidelberg, Berlin, Heidelberg, 2011) pp. 393–418.

[23] J. F. Babb, Journal of Physics: Conference Series **19**, 1.

[24] S. Y. Buhmann, *Dispersion Forces I: Macroscopic Quantum Electrodynamics and Ground-State Casimir, Casimir–Polder and van der Waals Forces* (Springer Berlin Heidelberg, Berlin, Heidelberg, 2012).

[25] S. Y. Buhmann, *Dispersion Forces II: Many-Body Effects, Excited Atoms, Finite Temperature and Quantum Friction* (Springer Berlin Heidelberg, Berlin, Heidelberg, 2012).

[26] S. G. Johnson, "Numerical methods for computing casimir interactions," in *Casimir Physics*, edited by D. Dalvit, P. Milonni, D. Roberts, and F. da Rosa (Springer Berlin Heidelberg, Berlin, Heidelberg, 2011) pp. 175–218.

[27] A. W. Rodriguez, P.-C. Hui, D. P. Woolf, S. G. Johnson, M. Lončar, and F. Capasso, Annalen der Physik **527**, 45 (2015).

[28] A. W. Rodriguez, F. Capasso, and S. G. Johnson, Nature Photonics **5**, 211 (2011).

[29] S. J. Rahi, T. Emig, N. Graham, R. L. Jaffe, and M. Kardar, Phys. Rev. D **80**, 085021 (2009).

[30] See supplemental information [url] for further details on the basis representation of the Green's function as well as an alternate derivation of the vdW interaction energy based on the fluctuation–dissipation theorem, which includes Refs. [48–52].

[31] R. H. French, V. A. Parsegian, R. Podgornik, R. F. Rajter, A. Jagota, J. Luo, D. Asthagiri, M. K. Chaudhury, Y.-m. Chiang, S. Granick, S. Kalinin, M. Kardar, R. Kjellander, D. C. Langreth, J. Lewis, S. Lustig, D. Wesolowski, J. S. Wettlaufer, W.-Y. Ching, M. Finnis, F. Houlihan, O. A. von Lilienfeld, C. J. van Oss, and T. Zemb, Rev. Mod. Phys. **82**, 1887 (2010).

[32] A. Lambrecht, P. A. M. Neto, and S. Reynaud, New Journal of Physics **8**, 243 (2006).

[33] M. T. H. Reid, J. White, and S. G. Johnson, Phys. Rev. A **88**, 022514 (2013).

[34] A. Rodriguez, M. Ibanescu, D. Iannuzzi, J. D. Joannopoulos, and S. G. Johnson, Phys. Rev. A **76**, 032106 (2007).

[35] A. W. Rodriguez, A. P. McCauley, J. D. Joannopoulos, and

S. G. Johnson, Phys. Rev. A **80**, 012115 (2009).
[36] A. P. McCauley, A. W. Rodriguez, J. D. Joannopoulos, and S. G. Johnson, Phys. Rev. A **81**, 012119 (2010).
[37] X. Ge and D. Lu, Phys. Rev. B **92**, 241107 (2015).
[38] A. G. Donchev, The Journal of Chemical Physics **125** (2006).
[39] J. Mahanty and B. W. Ninham, J. Chem. Soc., Faraday Trans. 2 **71**, 119 (1975).
[40] M. J. Renne, Physica **53**, 193 (1971).
[41] A. Mayer, Phys. Rev. B **75**, 045407 (2007).
[42] in *Principles of Nano-Optics* (Cambridge University Press, 2006) pp. 335–362.
[43] N. Ferguson, J. Becker, H. Tidow, S. Tremmel, T. D. Sharpe, G. Krause, J. Flinders, M. Petrovich, J. Berriman, H. Oschkinat, and A. R. Fersht, **103**, 16248 (2006).
[44] H. M. Berman, J. Westbrook, Z. Feng, G. Gilliland, T. N. Bhat, H. Weissig, I. N. Shindyalov, and P. E. Bourne, **28**, 235 (2000).
[45] H. Berman, K. Henrick, and H. Nakamura, Nat Struct Mol Biol **10**, 980 (2003).
[46] M. T. H. Reid and S. G. Johnson, IEEE Transactions on Antennas and Propagation **63**, 3588 (2015).
[47] `http://homerreid.com/scuff-EM`.
[48] F. S. S. Rosa, D. A. R. Dalvit, and P. W. Milonni, Phys. Rev. A **84**, 053813 (2011).
[49] G. S. Agarwal, Phys. Rev. A **11**, 243 (1975).
[50] T. B. MacRury and B. Linder, The Journal of Chemical Physics **58**, 5388 (1973).
[51] J. Mahanty and B. W. Ninham, Journal of Physics A: General Physics **5**, 1447.
[52] M. J. Renne, Physica **56**, 125 (1971).